

QPS TRANSPORT PHYSICS FLEXIBILITY USING VARIABLE COIL CURRENTS

DONALD A. SPONG,* DENNIS J. STRICKLER, STEVEN P. HIRSHMAN, JAMES F. LYON,
and LEE A. BERRY *Oak Ridge National Laboratory, P.O. Box 2009, Oak Ridge, Tennessee 37831-8073*

DAVID R. MIKKELSEN and DONALD A. MONTICELLO
Princeton Plasma Physics Laboratory, P.O. Box 451, Princeton, New Jersey 08502

ANDREW S. WARE *Department of Physics and Astronomy
University of Montana, Missoula, Montana 59812*

Received December 1, 2003

Accepted for Publication February 26, 2004

An important goal for a stellarator design is to incorporate enough flexibility to experimentally test a range of physics issues. The proposed Quasi-Poloidal Stellarator device achieves this by allowing independently variable currents in the modular, vertical field, and toroidal coil sets. Numerical optimizations and modeling show that this can allow significant tests of neoclassical cross-field transport rates, reduced poloidal flow damping (relative to the tokamak), and magnetic island width control. This flexibility is achieved in a unique, very low aspect ratio ($R_0/\langle a \rangle = 2.7$) two-field period (racetrack-shaped) configuration that generates rotational transform from a combination of internal plasma currents and external shaping.

KEYWORDS: *stellarator flexibility, neoclassical transport, magnetic island*

I. INTRODUCTION

Recently developed stellarator computational design tools¹ (STELLOPT code) have successfully merged the optimizations of external coils for engineering and internal plasma physics. This procedure controls the engineering features and complexity of the magnet coils, thus directly impacting the cost in an ongoing design. It also allows one to methodically explore the physics flexibility options in a completed design where the coil geometry is fixed, but where the coil currents can still be

*E-mail: spongda@ornl.gov

varied over some specified range. This type of flexibility is one of the significant advantages that stellarators can offer compared with tokamaks. Developing better tools for exploring the available parameter space can also enhance the scientific value of a stellarator experiment.

As an example of such flexibility studies, we analyze the Quasi-Poloidal Stellarator (QPS) device.² This is a very low aspect ratio ($R_0/\langle a \rangle = 2.7$) two-field period (racetrack-shaped) configuration that generates rotational transform from a combination of internal plasma currents and external shaping. The magnetic spectrum of QPS is dominantly poloidally symmetric with the highest degree of symmetry present near the magnetic axis (nonsymmetric mode energy = 0.062% of symmetric mode energy), dropping off to a lower degree of symmetry at the plasma edge (nonsymmetric mode energy = 3.25% of symmetric mode energy). This results from the QPS design criteria of keeping the neoclassical loss rates small compared with the expected anomalous losses, which also typically rise near the plasma edge. The physics goals of this device are to test equilibrium flux surface fragility and plasma confinement scaling at very low aspect ratio, to study plasma flow generation and damping under conditions where the viscous damping has a reversed ordering (poloidal viscosity < toroidal viscosity) from that of a tokamak, and to test ballooning/kink/vertical stability under first and possibly second stable regimes.³

QPS has been designed with independent power supplies for controlling the five unique modular coil groups, the three vertical field (VF) coil pairs, and the toroidal field (TF) coils. In addition, the plasma current can be controlled independently since an ohmic transformer is available to drive plasma current. Ten parameters can thus be independently varied. Since searches of even a ten-dimensional parameter space, based on intuition or

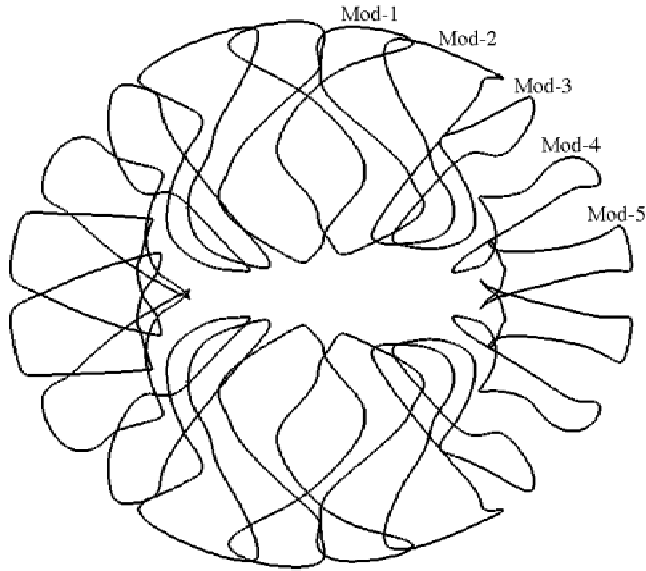


Fig. 1. Top view of QPS modular magnetic field coils. End coils are numbers 4 and 5 while 1, 2, and 3 are side coils.

trial and error, are likely to miss interesting combinations, we have used the merged coil-plasma optimizer code STELLOPT to automate this search process. In the following, we focus on transport improvement and island avoidance at low β , but such techniques can also be applied to the optimization of stability targets at finite β (Ref. 3).

II. COIL CONFIGURATION

The reference design for QPS is based on a set of 20 modular field coils (with 5 unique coil shapes), 6 VF coils, and 12 TF coils. In Fig. 1, the modular coils are shown from a top view, with the five unique coils labeled. The coil-current optimization will vary the currents in modular coils, VF coils, and the TF coils. Stellarator symmetry is maintained by keeping the currents in each unique modular coil group equal. A modular coil group consists of the modular coil that is present in

the first half of each field period along with its stellarator symmetric pair occurring in the second half of each field period. For QPS, each modular coil group contains four coils that will be run at the same current. Engineering constraints will limit the range over which these currents can be varied; the current constraints that we assume are listed in Table I. We will also constrain the currents to maintain approximately the same volume-averaged magnetic field among configurations. The current values given for the TF coil are for the total current flowing through the 12 TF coils; the other currents apply to individual coils. It should also be noted that in an experimental device some component of the VF coil currents is required for plasma positioning and compensation of stray fields from the ohmic transformer. We will not directly assess the latter current requirements in this study but will verify that the plasma-shape distortion does not become too large.

III. TRANSPORT OPTIMIZATION

As a first example of coil-current optimization, we will find current distributions that can either improve or degrade the neoclassical transport properties of QPS. A number of transport measures are available for this purpose, including the effective ripple (ϵ_{eff}) calculated from the NEO code⁴; collisional transport coefficients from the DKES code⁵; quasi-poloidal symmetry; and alignment of J^* (longitudinal adiabatic invariant),⁶ B_{min} , and B_{max} contours⁶ with flux contours. The primary target we will focus on in this paper is the effective ripple ϵ_{eff} . As will be shown, control of ϵ_{eff} has so far had the most direct correlation with other measures of transport such as DKES, global Monte Carlo lifetime estimates, and reductions in poloidal viscosity. We have also been able to directly improve quasi-poloidal symmetry by a factor of 4 to 5 over the reference design, but so far this has proven to be anticorrelated with other transport measures. This characteristic is possibly related to the particular solution that the optimizer finds for quasi-poloidal symmetry improvement, which is to increase currents in the corner section modular coils (Mod-4 and -5) and weaken currents in the side modular coils (Mod-2 and -3). This increases the ripple level and the fraction of trapped

TABLE I
Minimum, Maximum and Reference Current Levels for Our Flexibility Study

Coil	Mod-2	Mod-3	Mod-4	Mod-5	VF 1	VF 2	VF 3	TF
Minimum current (kA)	0	0	0	0	-60	-180	-130	-75
Maximum current (kA)	380	380	380	380	+60	+180	+130	+75
Reference design current (kA)	300	300	300	300	0	-75.5	-129	-24.9

particles and seems to have a stronger negative impact compared with any transport improvement arising from enhanced symmetry. Further work will be done on finding strategies for improving quasi-poloidal symmetry that are consistent with improvements in the other transport measures.

In Fig. 2 the values of effective ripple coefficients that have been obtained by targeting either improved or degraded transport are plotted as a function of the flux surface location. A significant variation (a factor of ~ 30) in low collisionality transport levels can be achieved over most of the plasma cross section by controlling coil currents. Table II gives the coil-current distributions that produce the configurations used in Fig. 2. As may be seen, lower ϵ_{eff} is obtained by raising the current in the middle Mod-2 coil and lowering it in the Mod-3, -4, and -5 coils comprising the corner section. To increase the effective ripple, the optimizer chooses to zero the current in the Mod-2 coil and increases currents in the Mod-1, -3, -4, and -5 coils up to their maximum limits. In Fig. 3 the variation of $|B|$ is plotted along a field line near the magnetic axis $[(\psi/\psi_{edge})^{1/2} = 0.06]$ for the three cases of Fig. 2. This shows that the primary effect leading to variations in low collisionality transport is the overall level of ripple in $|B|$. The degraded ϵ_{eff} case has the largest variation in $|B|$, while the improved case has the weakest variation in $|B|$. We have also found that the variation in $|B|$ on other flux surfaces going out to the plasma edge shows similar trends, as in Fig. 3. Coil-plasma separations have not been significantly changed

TABLE II

Coil Currents for Transport Optimized and Degraded Cases

	QPS Reference	NEO Optimized	NEO Deoptimized
Modular 1	3×10^5	3×10^5	3.8×10^5
Modular 2	3×10^5	3.29×10^5	0
Modular 3	3×10^5	2.12×10^5	3.8×10^5
Modular 4	3×10^5	2.78×10^5	3.8×10^5
Modular 5	3×10^5	2.79×10^5	3.8×10^5
Vertical 1	0	1×10^3	7.32×10^3
Vertical 2	-7.55×10^4	-5.62×10^4	-1.1×10^5
Vertical 3	-1.29×10^5	-1.3×10^5	-1.3×10^5
Toroidal	-2.49×10^4	-1.29×10^4	-1.45×10^4

by these optimizations; for the reference configuration, the minimum coil-plasma separation is 13.2 cm—it becomes 11.9 cm for the ϵ_{eff} -optimized case and 13.9 cm for the ϵ_{eff} -degraded case. These optimizations have been carried out using the Levenberg-Marquardt (LM) option of the STELOPT optimizer. Coil-current optimization attempts have also been made using differential evolution (DE) and genetic algorithm (GA) options. The DE and GA approaches allow the coil-current limits to be naturally incorporated into the calculation as bounds upon the search process but to date have not resulted in configurations with good flux surfaces. The LM algorithm does not provide any direct way to constrain the values

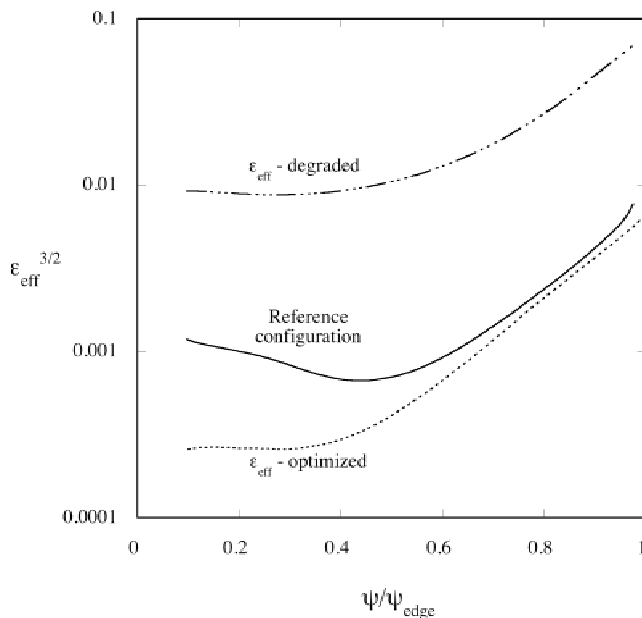


Fig. 2. Effective ripple coefficient as a function of normalized toroidal flux for the QPS reference configuration and for improved and degraded configurations.

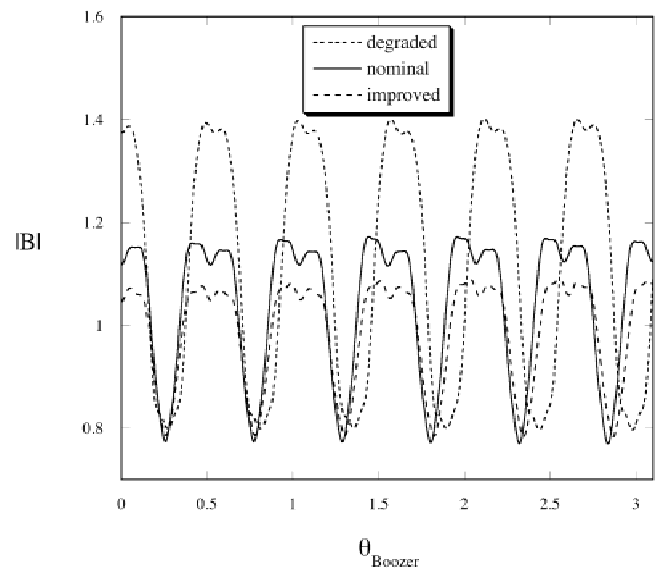


Fig. 3. Variation of $|B|$ (in Tesla) along a field line for a flux surface near the magnetic axis $[(\psi/\psi_{edge})^{1/2} = 0.06]$ for the reference ϵ_{eff} -optimized and ϵ_{eff} -degraded cases of Fig. 2.

accessed by coil currents and therefore requires constraint-related targets to accomplish this. Typically, one runs the LM method for a certain number of iterations, finds that one or more of the coil currents has gone outside of its acceptable range, fixes these coil currents at whichever bound is closest (i.e., maximum/minimum value), restarts the LM algorithm using the reduced number of coils, checks again, etc.

The effectiveness of the above optimization/de-optimization of transport has been further checked by using other measures of transport. We have run the DKES code,⁵ which calculates collisional transport coefficients, and the DELTA5D Monte Carlo code,⁷ which calculates global energy lifetimes. In Fig. 4 the DKES monoenergetic particle and energy cross-field transport coefficients are plotted versus the DKES collisionality parameter (ν/ν) for a half-radius flux surface and with no radial electric field $E_r = 0$ (to emphasize configurational differences). Here, $r = \langle a \rangle (\psi/\psi_{edge})^{1/2}$ is a dimensional (in meters) flux surface label. At low collisionalities (below plateau values corresponding to $\nu/\nu < 0.02$), these show similar variations with optimization as does the effective ripple coefficient shown in Fig. 2. In the higher collisionality regime, there is not as much sensitivity to the configuration (as one would expect since local variations in $|B|$ do not lead to different classes of trapped particles in the short mean-free-path regime). Figure 5 shows the Monte Carlo ion energy lifetimes for the reference ϵ_{eff} -degraded and ϵ_{eff} -optimized configurations corresponding to the plasma parameters: $T_{electron}(0) =$

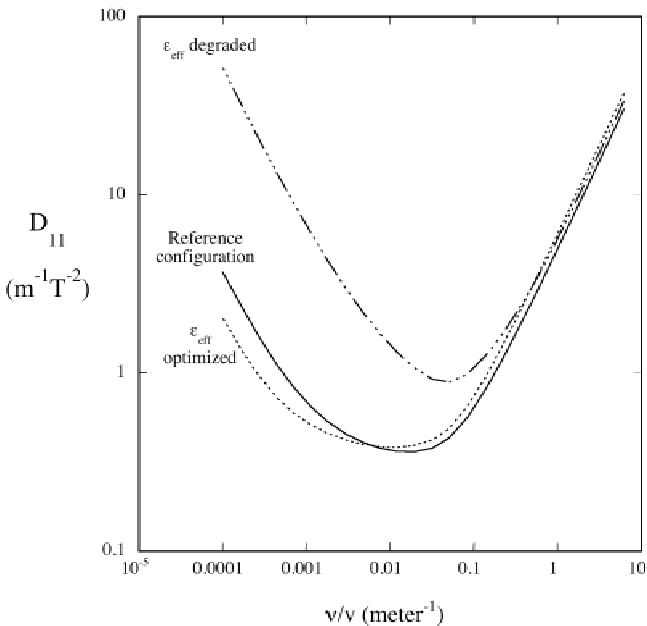


Fig. 4. DKES monoenergetic transport coefficient versus collisionality for the reference, effective ripple optimized, and degraded cases (for $E_r = 0$).

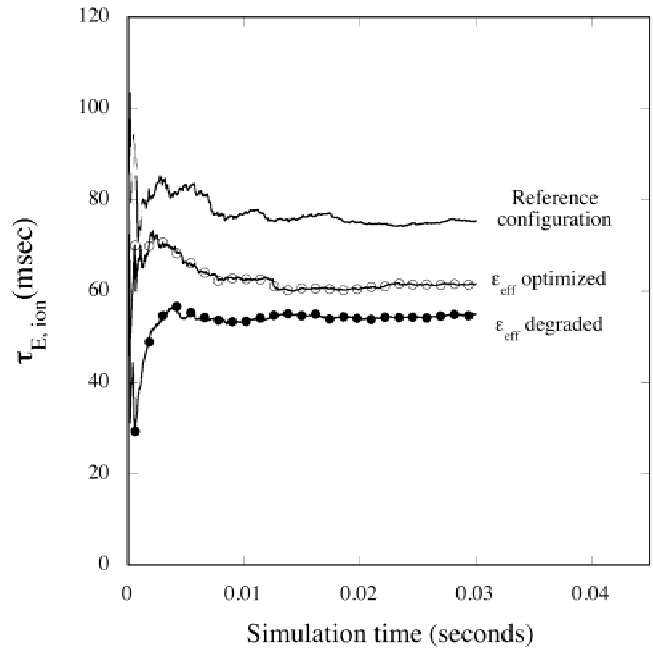


Fig. 5. Monte Carlo global ion energy lifetimes ($E_r = 0$) for reference, transport-degraded, and optimized configurations based on parameters typical of the QPS ICRF heated scenario.

0.5 keV, $T_{ion}(0) = 0.5$ keV, and $n(0) = 8.3 \times 10^{19} \text{ m}^{-3}$. These parameters are expected to be typical of the QPS with ion cyclotron resonance heating (ICRH). Figure 5 indicates that the ϵ_{eff} -optimized configuration has lifetimes in between the reference and ϵ_{eff} -degraded configurations. There is also some tendency toward this behavior in the plateau and higher collisionalities of Fig. 4. The differing trends between the NEO/DKES results of Figs. 2 and 4 and the Monte Carlo lifetimes are probably related to the different physics content of the two calculations. The Monte Carlo lifetimes do not assume diffusive transport but rather take into account transport properties over the entire volume and are based on a Maxwellian distribution; the DKES results of Fig. 4 are monoenergetic and evaluated at a fixed flux surface. Nevertheless, both measures show that a significant variation in confinement can be accessed by coil-current variations.

In addition to cross-field particle and energy transport, flow damping and flow generation effects are also important issues for compact stellarators. Sheared flows are expected to play a pivotal role in turbulence suppression and in the generation of transport barriers. In addition, the diagnosis and control of impurity transport depends on the inclusion of multiple species in the momentum balance relation and prediction of impurity flow velocities.

Recent methods developed by Sugama and Nishimura⁸ have allowed a momentum conserving calculation of the neoclassical viscosity tensor for a stellarator based

upon the transport coefficients obtained from the DKES code. The ability to implement this procedure is currently hampered at low collisionalities by the reduced convergence of DKES. Also, at high electric fields and collisionalities, flows are expected to depart from the incompressible approximation.^{8,9} However, the range of applicability between these limits is generally sufficient so as to provide us with at least qualitative indications of the different flow damping physics present in a quasi-poloidal device as compared to the equivalent toroidally symmetric device.

In a perfectly symmetric quasi-poloidal device, the poloidal viscous damping would go to zero, and any non-zero parallel flow components (V_{\parallel}) would be canceled out by the generation of a counteracting toroidal $E \times B$ drift component ($E_r \times B_p$) leading to the relation $E_r = (B_t/B_p)BV_{\parallel}$ between the parallel flow and the electric field ($B_p, B_t =$ poloidal/toroidal magnetic field components). This implies that the radial electric field in QPS will be larger by $\sim(B_t/B_p)^2$ compared with the equivalent relation in a perfectly symmetric tokamak $E_r = B_p V_{\parallel}$, where the poloidal flow components must cancel (due to the vanishing of the toroidal viscous damping). In a realistic quasi-poloidal system, there will be somewhat larger damping of the parallel flows due to the higher level of parallel viscosity (see Fig. 6b) but not by a large enough factor in the plateau regime $\nu/\nu \sim 0.01$ (relevant to ion flows) to negate the $(B_t/B_p)^2$ enhancement factor. This larger radial electric field should also reduce the radial diffusivity in QPS.

The basis for the dominance of poloidal flows in QPS is also seen in Fig. 6a where the monoenergetic poloidal viscosity coefficient is reduced by up to a factor of 10 in the plateau regime from that for the equivalent tokamak (i.e., the tokamak with the same iota profile and toroidally averaged shape as QPS). The coefficients plotted in Fig. 6 are related to those of Ref. 8 by

$$\mu_{\theta\theta} = M_{aPP}(K)/m\nu_T K^{3/2},$$

$$\mu_{\parallel} = M^* = M_a(K)/m\nu_T K^{3/2},$$

where $K = (\nu/\nu_T)^2$ and $\nu_T = (2kT/m)^{1/2}$; M_{aPP} and M^* are defined in Eqs. (B5) and (54) of Ref. 8. In evaluating the viscosity coefficient expressions of Ref. 8, we have used DKES coefficients calculated at the $\psi/\psi_{edge} = 0.25$ surface and have used the relation¹⁰

$$\langle \tilde{U}^2 \rangle = \frac{3}{2} \frac{D_{11}}{\nu/\nu} \quad \left(\text{evaluated for } \nu/\nu \text{ in the Pfirsch-Schlüter regime} \right)$$

to obtain the required flux surface-average-squared Pfirsch-Schlüter velocity. These characteristics of quasi-poloidal systems lead us to conclude that it should be possible to control the electric field level and the shear with less momentum input than for a similar axisymmetric system.

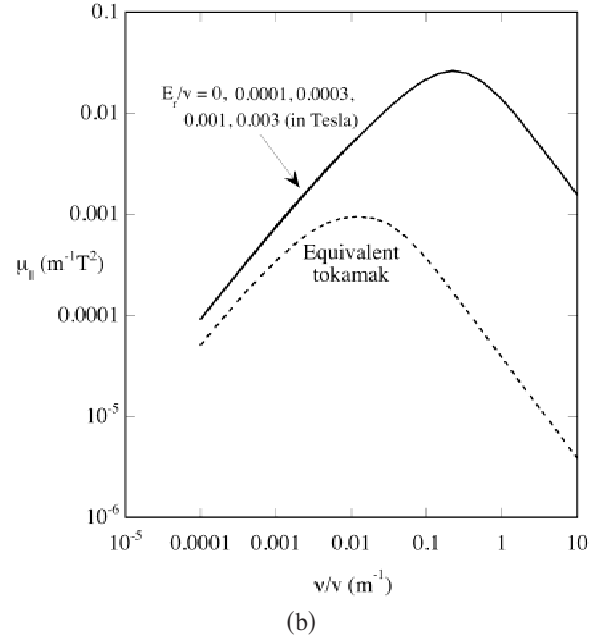
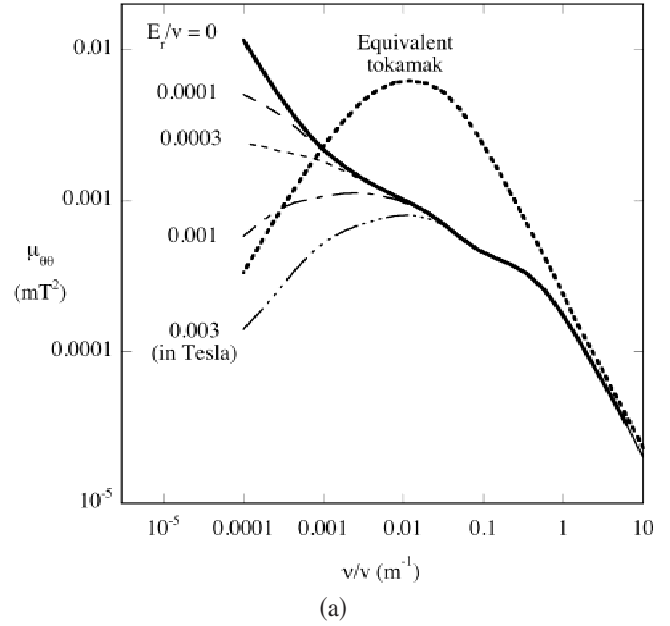
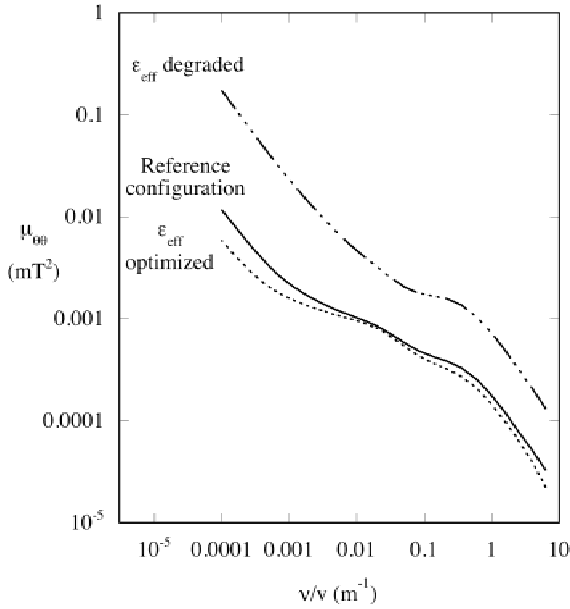
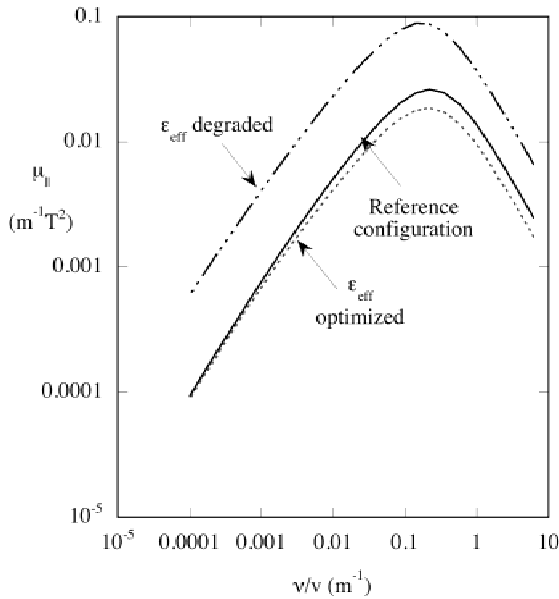


Fig. 6. Monoenergetic (a) poloidal and (b) parallel neo-classical viscosities versus collisionality and ambipolar electric field for the QPS configuration, evaluated at $\psi/\psi_{edge} = 0.25$. These are obtained using the DKES code⁵ coupled with the analysis of Sugama and Nishimura.⁸

The viscous coefficients plotted in Figs. 6 can also be modified by variations in coil currents in a similar way as the effective ripple and cross-field transport coefficients plotted in Figs. 2 and 4. In Figs. 7 we plot the monoenergetic poloidal and parallel viscous coefficients (for $E_r = 0$ and $\psi/\psi_{edge} = 0.25$) using the effective ripple



(a)



(b)

Fig. 7. Range of flexibility in (a) poloidal and (b) parallel neoclassical viscosities versus collisionality based on the effective ripple ϵ_{eff} optimization studies shown in Fig. 2. These are evaluated at $\psi/\psi_{edge} = 0.25$ and for $E_r = 0$.

optimized and degraded coil-current distributions that were mentioned earlier. We conclude that the poloidal viscosity can be varied by a factor of ~ 10 while the parallel viscosity can be varied by a factor of 2 to 3. These coefficients have not been directly targeted by the optimization yet, but this may be the topic of future research.

IV. ISLAND AVOIDANCE

In addition to variations in the coil currents for confinement optimization, we have carried out optimizations to control the shape of the rotational transform profile. The goal has been to use combinations of ohmically driven plasma current and modifications in the coil-current distributions to keep the iota profile in a range bounded between values determined by adjacent low-order rational surfaces (which occur for QPS at $iota = 2/8, 2/7, 2/6, 2/5, \text{etc.}$). Once such configurations are found, they are checked by the PIES code¹¹ for magnetic islands. If good surfaces are found, then the search ends; if large islands are present, further optimizations are performed to avoid the offending resonances in the plasma. As there is generally some deviation between the rotational transform predicted by VMEC and that given by PIES, several iterations of this process may be required to find a satisfactory configuration. In the operation of low aspect ratio stellarator devices, this type of search for optimum plasma and coil-current distributions for island avoidance is expected to be of importance in finding attractive regimes of operation. It may also be possible to more directly target island reduction through targeting measures such as normal magnetic field components, parallel currents, and resonant Jacobian Fourier components at the island locations.

We have optimized vacuum configurations with most of the weight placed on the target for attaining a specific rotational transform profile. For the results presented here, the transport properties have then been checked a posteriori, indicating that in addition to decreased island sizes, the new configurations generally lead to improved confinement. The coil-current optimizations have been carried out with varying levels of ohmic current present; the ohmic-current profile has been modeled as centrally peaked. By combining the coil-current optimization with finite plasma currents, we have been able to both raise the rotational transform and flatten it at the same time.

Figure 8 shows some of the VMEC rotational transform profiles that we have obtained by this procedure. Out of these profiles, the one with 25 kA has resulted in the best magnetic surfaces. The 37-kA profile generated 4/11 islands that destroyed the outer part of the plasma while the 12-kA case generated 2/7 islands. However, with further iterations between the optimizer and PIES, it should also be possible to avoid major islands in the 12- and 37-kA cases. Table III shows the coil-current distributions that were used to produce the above cases; note that the 12- and 25-kA cases use the same coil currents—only the plasma current has been changed. In Fig. 9, the surfaces obtained from the PIES code are shown for the 25-kA case, indicating that island widths have been made small by this procedure. The 25-kA optimized case had a minimum coil-plasma separation of 14.6 cm as compared with 13.2 cm in the reference case. In Fig. 10 global ion energy lifetimes as obtained from Monte Carlo

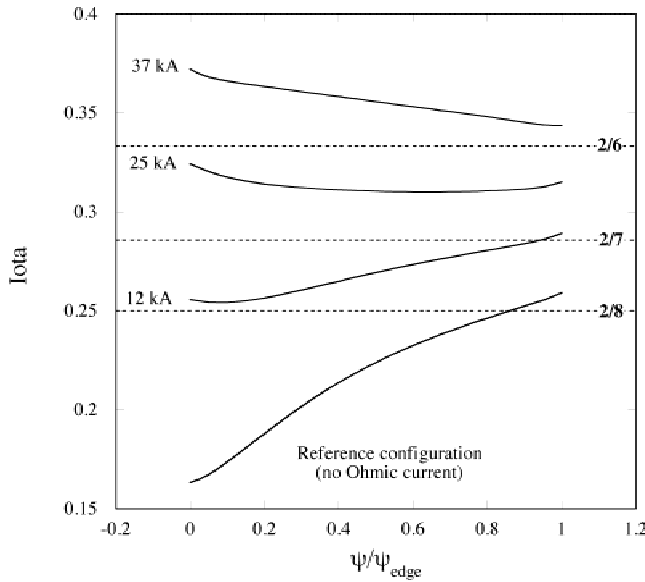


Fig. 8. QPS rotational transform profiles that have been attained through combinations of ohmic plasma current and coil-current optimization.

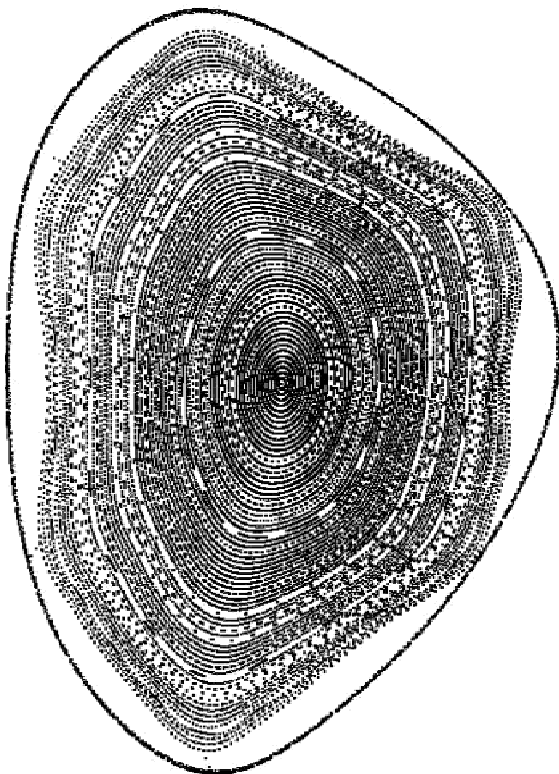


Fig. 9. PIES magnetic surfaces for the coil-current optimized case with 25 kA. The transform profile is constrained to remain between the 2/6 and 2/7 resonances.

TABLE III

Coil Currents for the Rotational Transform Profiles Shown in Fig. 8

	QPS Reference	12- and 25-kA Cases	37-kA Case
Modular 1	3×10^5	3.56×10^5	3.65×10^5
Modular 2	3×10^5	3.57×10^5	3.47×10^5
Modular 3	3×10^5	3.42×10^5	3.79×10^5
Modular 4	3×10^5	2.86×10^5	3.75×10^5
Modular 5	3×10^5	3.52×10^5	3.41×10^5
Vertical 1	0	1.58×10^4	5.79×10^4
Vertical 2	-7.55×10^4	-1.8×10^5	8.91×10^4
Vertical 3	-1.29×10^5	-1.19×10^5	1.24×10^5
Toroidal	-2.49×10^4	-5.2×10^4	-3.56×10^4

calculations for the QPS ion cyclotron range of frequency (ICRF) heated scenario are shown for the four rotational transform profiles of Fig. 8. These indicate that the rotational transform profile can be varied with relatively little influence (10 to 15% variation) on the ion energy confinement.

V. CONCLUSIONS

Physics flexibility is an important aspect of stellarator experiments. We have demonstrated a technique to methodically search for configurations that sample

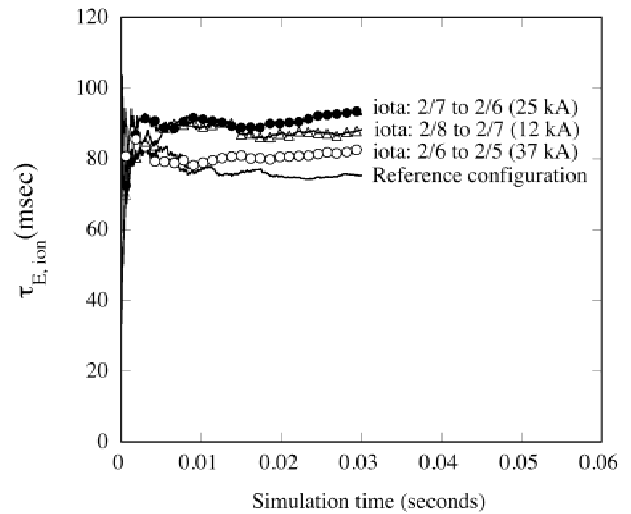


Fig. 10. Monte Carlo global ion energy lifetimes ($E_r = 0$) for the different rotational transform profiles of Fig. 8 based on parameters typical of the QPS ICRF heated scenario.

extremes of transport and that minimize low β islands using the STELLOPT optimizer. This approach is especially useful when individual modular coil group currents can be varied as well as VF and TF coil currents. In the case of the QPS device, coil-current distributions have been found that result in up to a factor of ~ 30 variation in low collisionality transport. Also, the transform profile can be regulated to remain between adjacent rationals, resulting only in island chains of very limited width. Similar techniques should be applicable to other optimization targets, such as stability.

ACKNOWLEDGMENTS

This work was supported by the U.S. Department of Energy under contract DE-AC05-00OR22725 with UT-Battelle, LLC. The calculations in this paper have been carried out using the resources of the National Energy Research Scientific Computing Center, the Lawrence Berkeley National Laboratory, and the Center for Computational Sciences at Oak Ridge National Laboratory.

REFERENCES

1. D. J. STRICKLER et al., "Development of a Robust Quasi-Poloidal Compact Stellarator," *Fusion Sci. Technol.*, **45**, 15 (2004).
2. J. F. LYON et al., "Overview of the QPS Project," *Proc. 30th Conf. Controlled Fusion and Plasma Physics*, St. Petersburg, Russia, July 7–11, 2003, European Physical Society (2003); see also D. A. SPONG et al., "Confinement Physics of Quasi-Poloidal Stellarators," *Proc. 30th Conf. Controlled Fusion and Plasma Physics*, St. Petersburg, Russia, July 7–11, 2003, European Physical Society (2003).
3. A. A. WARE et al., *Phys. Plasmas* (2003) (submitted for publication).
4. V. V. NEMOV, S. V. KASILOV, W. KERNBICHLER, and M. F. HEYN, "Evaluation of $1/\nu$ Neoclassical Transport in Stellarators," *Phys. Plasmas*, **6**, 4622 (1999).
5. W. I. VAN RIJ and S. P. HIRSHMAN, "Variational Bounds for Transport Coefficients in Three-Dimensional Toroidal Plasmas," *Phys. Fluids B*, **1**, 563 (Mar. 1989).
6. J. A. ROME, "Orbit Topology in Conventional Stellarators in the Presence of Electric Fields," *Nucl. Fusion*, **35**, 195 (1995).
7. D. A. SPONG et al., *Nucl. Fusion*, **41**, 711 (2001).
8. H. SUGAMA and S. NISHIMURA, "How to Calculate the Neoclassical Viscosity, Diffusion, and Current Coefficients in General Toroidal Plasmas," *Phys. Plasmas*, **9**, 4637 (2002).
9. H. MAASSBERG et al., "The Neoclassical "Electron Root" Feature in the Wendelstein-7-AS Stellarator," *Phys. Plasmas*, **7**, 295 (2000).
10. H. SUGAMA, Personal Communication.
11. A. REIMAN and H. S. GREENSIDE, *J. Comput. Phys.*, **75**, 423 (1988).

Donald A. Spong (BS, nuclear engineering, University of Arizona, 1970; MSE, 1971, and PhD, 1976, nuclear engineering, University of Michigan) is a senior research staff member and stellarator theory group leader in the Fusion Energy Division at Oak Ridge National Laboratory (ORNL). His research interests include stellarator neoclassical transport, stellarator optimization, particle simulation of energetic populations, Alfvén instabilities magnetohydrodynamics in three-dimensional (3-D) systems, and flux surface fragility in compact stellarators.

Dennis J. Strickler (BA, mathematics, Berea College, 1971; MA, mathematics, University of Kentucky, 1973) is a research staff member in the Computational Sciences and Engineering Division at ORNL. His responsibilities and research interests are in the area of magnetic coil design for compact stellarators.

Steven P. Hirshman [EE and MS, 1973, and ScD, 1976, electrical engineering, Massachusetts Institute of Technology (MIT)] is a senior research staff scientist in the Fusion Energy Division at ORNL. His research interests include theoretical modeling and simulation of equilibrium and transport in 3-D toroidal plasma configurations.

James F. Lyon (BS and MS, electrical engineering, MIT, 1964; PhD, physics, University of Tennessee, 1970) is the stellarator program coordinator in the Fusion Energy Division at ORNL, where he serves as Quasi-Poloidal Stellarator (QPS) project head, National Compact Stellarator Experiment (NCSX) deputy project manager, and Large Helical Device experimentalist. His research

interests are in stellarator physics and design, reactor systems optimization, fast ion measurements, and flux surface calculations.

Lee A. Berry (BA, MA, and PhD, University of California, Riverside) is a senior research staff scientist in the Fusion Energy Division at ORNL. His current research interests are in radio-frequency theory and modeling, stellarator physics and design, and computer-based modeling.

David R. Mikkelsen (BS, physics, California Institute of Technology, 1971; PhD, physics, University of Washington, 1975) is a principal research physicist at the Princeton Plasma Physics Laboratory (PPPL). His research interests include neoclassical transport in stellarators and turbulent transport in tokamaks.

Donald A. Monticello (BS, University of Rochester, 1963; PhD, University of Rochester, 1973) is a principal research physicist at PPPL. His research interests include development of the PIES (Princeton Interactive Equilibrium Solver) code and 3-D equilibrium.

Andrew S. Ware (BS, physics, University of Texas, 1988; PhD, physics, University of California, San Diego, 1992) is an associate professor of physics at the University of Montana. His research interests include the equilibrium and stability of stellarator plasmas, plasma turbulence and turbulent transport, and turbulence in geophysical fluids.